0026-895X/09/7601-105–112$20.00
MOLECULAR PHARMACOLOGY
Copyright © 2009 The American Society for Pharmacology and Experimental Therapeutics
Mol Pharmacol 76:105–112, 2009

Vol. 76, No. 1
53744/3489989
Printed in U.S.A.

Inhibition of Aquaporin-1 and Aquaporin-4 Water Permeability by a Derivative of the Loop Diuretic Bumetanide Acting at an Internal Pore-Occluding Binding Site

Elton Migliati, Nathalie Meurice, Pascale DuBois, Jennifer S. Fang, Suma Somasekharan, Elizabeth Beckett, Gary Flynn, and Andrea J. Yool

Discipline of Physiology, School of Molecular and Biomedical Science, University of Adelaide, Adelaide, Australia (A.J.Y., E.B., P.D.); Physiological Sciences Program, University of Arizona, Tucson, Arizona (A.J.Y., E.M., J.S.F.); College of Pharmacy & BIO5 Institute, University of Arizona, Tucson, Arizona (N.M., G.F.); Chemogenomics Laboratory, Translational Genomics Research Institute (TGen), Phoenix, Arizona, and FRS-FNRS, Laboratoire de Physico-Chimie Informatique, University of Namur, Namur, Belgium (N.M.); and Department of Cellular & Molecular Physiology, Yale University, New Haven, Connecticut (S.S.)

Received November 26, 2008; accepted April 23, 2009

ABSTRACT

Aquaporin (AQP) water channels, essential for fluid homeostasis, are expressed in perivascular brain end-feet regions of astroglia (AQP4) and in choroid plexus (AQP1). At a high concentration, the loop diuretic bumetanide has been shown to reduce rat brain edema after ischemic stroke by blocking Na^+-K^+-$2Cl^-$ cotransport. We hypothesized that an additional inhibition of AQP contributes to the protection. We show that osmotic water flux in AQP4-expressing *Xenopus laevis* oocytes is reduced by extracellular bumetanide (≥100 μM). The efficacy of block by bumetanide is increased by injection intracellularly. Forty-five synthesized bumetanide derivatives were tested on oocytes expressing human AQP1 and rat AQP4. Of these, one of the most effective was the 4-aminopyridine carboxamide analog, AqB013, which inhibits AQP1 and AQP4 (IC_{50} ~20 μM, applied extracellularly). The efficacy of block was enhanced by mutagenesis of intracellular AQP4 valine-189 to alanine (V189A, IC_{50} ~8 μM), confirming the aquaporin as the molecular target of block. In silico docking of AqB013 supported an intracellular candidate binding site in rat AQP4 and suggested that the block involves occlusion of the AQP water pore at the cytoplasmic side. AqB013 at 2 μM had no effect, and 20 μM caused 20% block of human Na^+-K^+-$2Cl^-$ cotransporter activity, in contrast to >90% block of the transporter by bumetanide. AqB013 did not affect *X. laevis* oocyte Cl^- currents and did not alter rhythmic electrical conduction in an ex vivo gastric muscle preparation. The identification of AQP-selective pharmacological agents opens opportunities for breakthrough strategies in the treatment of edema and other fluid imbalance disorders.

Aquaporin channels, members of the major intrinsic protein family found in prokaryotes and eukaryotes (Reizer et al., 1993; Hohmann et al., 2000), are essential for maintaining fluid homeostasis and enabling the movement of water and other solutes across barrier membranes in tissues throughout the body (Agre et al., 1993). In the mammalian brain, AQP4 water channels are expressed in astroglial cells at the blood-brain-barrier interface, and AQP1 channels are expressed in choroid plexus for cerebral spinal fluid secretion (Yool, 2007a). In conditions of injury, AQPs enhance short-term vulnerability to pathological volume changes and promote edema formation (Manley et al., 2000; Amiry-Moghaddam et al., 2004a).

Inhibitors of aquaporins with translational potential are needed. Blockers found thus far are handicapped by toxicity, low efficacy, and lack of specificity. Mercurials block certain classes such as AQP1 (Preston et al., 1993) but not AQP4 (Jung et al., 1994a), but toxicity limits therapeutic value. Antiepileptic compounds (Huber et al., 2009), acetazolamide (Ma et al., 2004), and metal ions (Niemietz and Tyerman, 2002) also have been proposed as AQP inhibitors. The nonmercurial AQP1 blocker, tetraethylammonium ion (TEA^+), decreases AQP1-mediated water fluxes in the oocyte expression system (Brooks et al., 2000; Det-

This work was supported by the National Institutes of Health National Institute of General Medical Sciences [R01-GM059986]; University of Arizona BIO5 Pilot Grant; the University of Adelaide School of Molecular and Biomedical Science; and the Belgian National Fund for Scientific Research Fonds de la Recherche Scientifique–Fonds National de la Recherche Scientifique Postdoctoral fellowship.

E.M. and N.M. contributed equally to this work and should be considered co-first authors.

Article, publication date, and citation information can be found at http://molpharm.aspetjournals.org.

doi:10.1124/mol.108.053744.

ABBREVIATIONS: AQP, aquaporin; NKCC1, Na^+-K^+-$2Cl^-$ cotransporter; TEA, tetraethylammonium; DMSO, dimethyl sulfoxide; MOE, Molecular Operating Environment; KRB, Krebs-Ringer-bicarbonate.

mers et al., 2006) and in the kidney (Yool et al., 2002). TEA block of AQPs is supported by molecular dynamic modeling (Muller et al., 2008), although is not seen in all assays (Yang et al., 2006). TEA also blocks a variety of K^+ channels and other membrane proteins.

In our initial screen of various channel and transporter blockers, bumetanide showed a modest blocking effect on AQP-mediated osmotic swelling in *X. laevis* oocytes. Bumetanide, furosemide, and torsemide are loop diuretic drugs that block Na^+-K^+-$2Cl^-$ cotransport in the kidney. Further consideration of bumetanide was supported by a link to edema; prior work of O'Donnell and colleagues showed that bumetanide exerts a protective effect in rodent brain edema by a mechanism independent of renal diuretic activity (O'Donnell et al., 2004; Lam et al., 2005). Although the benefit of Na^+ cotransport inhibition in brain edema is clearly established, we hypothesized that an additional inhibitory effect of a high dose of bumetanide on AQP might augment the protective effect in vivo. As a generically prescribed loop diuretic, bumetanide represents an attractive scaffold for medicinal chemistry efforts. Systemic bumetanide is tolerated without overt toxicity at doses as high as 100 mg/kg (short- and long-term administration) in species including rat, rabbit, dog, and baboon (McClain and Dammers, 1981).

Edema commands clinical attention in neurological, pulmonary, and other life-threatening conditions. The extent of brain edema after injury or stroke is a major determinant of survival, yet limited treatments are available to patients with massive brain edema. Molecular tools for intervention in edema are needed, but discovery of agents that modulate brain aquaporin channels and are tractable for medicinal chemistry has proven elusive. The strategic position of AQP4 in brain perivascular glial end-feet makes it a target for intervention in edema formation. We show here that a compound, AqB013, structurally related to the loop diuretic bumetanide, blocks mammalian AQP1 and AQP4 channels in the *X. laevis* oocyte expression system. Our results indicate that the block by AqB013 is at an intracellular site that occludes the water pore.

This discovery of a first-in-class AQP blocker, AqB013, and its candidate binding site opens a new area of research that could have significant translational applications in brain, lung, and heart edema, glaucoma, cancer, renal dysfunction, and other conditions involving alterations in volume, transport, and fluid homeostasis in AQP-expressing tissues (Yool, 2007b). In ongoing work, the translation of these findings to in vivo models of disease will be the essential next step for developing new strategies for intervention.

Materials and Methods

Oocyte Preparation. Unfertilized *X. laevis* oocytes were defolliculated with collagenase (type1A, 1.5 mg/ml; Sigma, St. Louis, MO) and trypsin inhibitor (15 mg/ml) in OR-2 saline (82 mM NaCl, 2.5 mM KCl, 1 mM $MgCl_2$, and 5 mM HEPES) at 18°C for 1.5 h, washed in OR-2 saline solution, and held in isotonic culture saline [96 mM NaCl, 2 mM KCl, 0.6 mM $CaCl_2$, 5 mM $MgCl_2$, and 5 mM HEPES with 10% horse serum (Invitrogen, Carlsbad CA), 100 U/ml penicillin, and 100 μg/ml streptomycin, pH 7.6]. Oocytes were injected with 50 nl of water containing 1 to 4 ng of cRNA for AQP1 or AQP4 and were incubated for 2 to 5 days at 18°C.

RNA Preparation. Rat AQP4 and human AQP1 cDNAs (provided by P. Agre, The Johns Hopkins University, Baltimore, MD) subcloned into a *X. laevis* β-globin plasmid were linearized with BamHI and transcribed in vitro (T3 mMessage mMachine; Ambion Inc., Austin, TX). cRNA was resuspended in sterile water. Site-directed mutations (QuikChange; Stratagene, La Jolla, CA) without introduced errors were confirmed by DNA sequencing.

Quantitative Swelling Assay. For standard assays, oocytes were incubated with or without drugs in isotonic saline (without serum or antibiotics) for 1 to 2 h at room temperature and were tested for swelling in 50% hypotonic saline (isotonic diluted with an equal volume of water without drug present). To compile results from multiple batches, data were standardized as a percentage of the mean swelling rate of untreated wild-type AQP-expressing oocytes on the same day. For double-swelling assays, each oocyte served as its own control and was assayed first without drug treatment, incubated for 1 to 2 h in isotonic saline with or without drug, and reassessed in a second swelling assay.

Swelling rates were quantified by relative increases in oocyte cross-sectional area imaged by videomicroscopy (charge-coupled device camera; Cohu, San Diego, CA) at 0.5 frames per second for 40 s using NIH ImageJ software. Rates were measured as slopes of linear regression fits using Kaleidagraph (Synergy Software, Reading, PA) or Prism (GraphPad Software Inc., San Diego, CA). Dose-response curves were fit by the function percentage block = $(B_{max})(C)/(IC_{50} + C)$, where B_{max} is the maximum percentage block, and C is the concentration of drug in the extracellular incubation saline between paired swelling assays.

Bumetanide, furosemide (Sigma), and AqB013 (G. Flynn, Spacefill Enterprises, LLC, Tucson, AZ) were prepared as stock solutions (100 mM) in dimethyl sulfoxide (DMSO) and stored at 4°C. Experimental solutions of $\leq$100 μM final concentration were made by slow addition of the DMSO stock into a final volume of isotonic saline during rapid mixing. For concentrations >100 μM, drugs were sonicated in saline with 0.1% DMSO final. Oocytes incubated in vehicle saline with 0.1% DMSO alone showed no significant difference from control.

NKCC1 Flux Assays. Assays of human Na^+-K^+-$2Cl^-$ cotransporter activity were done using methods described previously (Darman and Forbush, 2002). In brief, Na^+-K^+-$2Cl^-$ cotransporter activity was measured from ^{86}Rb influx (PhosphorImager; GE Healthcare, Chalfont St. Giles, Buckinghamshire, UK) into a confluent monolayer of human embryonic kidney 293 cells expressing human NKCC1 in an automated 96-well plate flux machine (Fluxomatic; B. Forbush III, Yale University, New Haven, CT). Cells were preincubated for 45 min in low Cl^- hypotonic medium (substituted with gluconate) to activate the transporter and then subjected to a 1-min ^{86}Rb influx assay, with and without pharmacological compounds (200 μM bumetanide, 2 μM AqB013, 20 μM AqB013) added to the flux medium (135 mM NaCl, 5 mM RbCl, 1 mM $CaCl_2$, 1 mM $MgCl_2$, 1 mM Na_2HPO_4, 1 mM Na_2SO_4, and 15 mM sodium-HEPES, pH 7.4, with ~1 μCi/ml ^{86}Rb and 10^{-4} M ouabain). Virtually all of the ouabain-insensitive ^{86}Rb influx in these cells is bumetanide-sensitive (Darman and Forbush, 2002). Data points for each treatment were based on 12 replicate wells per plate; the transport assays were repeated in four separate experiments ($n = 4$).

Statistical Analyses. Histograms show mean ± S.E.M. For box plots, the box comprises 50% of data, the horizontal bar indicates median value, and error bars illustrate the full range. Statistical analyses were done with one-way analysis of variance, followed by post hoc Bonferroni tests (unless otherwise indicated), with statistical significance indicated as *, $p < 0.05$, and **, $p < 0.001$ (Prism).

Molecular Modeling. At the onset of our studies, the electron crystal structure of human AQP4 (2D57) had not been reported. Therefore, a homology model of rat AQP4 was constructed from the available bovine AQP1 structure (1J4N). Molecular modeling simulations were performed with Molecular Operating Environment (MOE) software (versions 2004.03, 2005.06, and 2007.0902; available at http://www.chemcomp.com; Chemical Computing Group Inc., Montreal, QC, Canada). MOE-align and -homology were used for

protein sequence alignment of eight AQP1 and two AQP4 mammalian sequences and for homology modeling of rAQP4 based on AQP1 crystal structure (Protein Data Bank ID 1J4N). Thirty-four terminal out-gaps of rAQP4 were omitted by excluding distal segments before Phe34 and after Ser267. Backbone geometry of the prototype model was refined where needed by adjusting main-chain atoms and minimizing energies. Binding site identification in the theoretical rAQP4 model was carried out using the Alpha Site Finder tool, implemented in MOE using default parameters including probe radii and distance cutoffs. The Site Finder geometric analysis is based on Alpha Shapes, a generalization of convex hulls (Edelsbrunner et al., 1995) that produces clusters of Alpha Spheres with hydrophobic or hydrophilic properties, which were used for molecular docking simulations and hypothesis generation for candidate binding sites. Ligands conformations were generated before docking using a stochastic conformational search. Nonredundant conformers were clustered, selected for lowest energy conformations, and used as input for molecular docking runs. Alpha triangle was used as a docking placement methodology and London dG as initial scoring function. Refined poses were rescored using the London dG function and further characterized by GB/VI and interaction energies. Thirty poses per docked conformer were refined, rescored, and optimized in MMFF94x and then manually curated and prioritized based on the energy of interaction, predicted H-bonds, and predicted pK_i.

Organic Chemical Syntheses. Standard methods were used to prepare analogs of bumetanide via an imidazolide intermediate. Purified products were characterized by nuclear magnetic resonance and mass spectroscopy. Proton and carbon NMR spectra were obtained on a Bruker 300 MHz instrument (Bruker, Newark, DE).

To prepare the imidazolide of bumetanide, 1,1-carbonyldiimidazole (2.95 mmol) was added to a solution of bumetanide (2.49mmol) and 15 ml of ethyl acetate EtOAc (at 25°C under argon). The mixture was heated until homogeneous, and a white precipitate formed on cooling. Thin-layer chromatography (silica gel 60 F254) using 100% EtOAc showed no bumetanide remaining. The precipitate was isolated by vacuum filtration, washed with EtOAc, and vacuum-dried under argon to obtain 1.05 g (approximately 99% yield) of white powder: ^{1}H and ^{13}C NMR in $CDCl_3$ were consistent with the product. The following results were obtained while verifying the preparation of the imidazole of bumetanide: ^{1}H NMR (300 MHz, $CDCl_3$): 0.82 (t, J = 7.5 Hz, 3H), 1.14 (m, J = 7.5 Hz, 2H), 1.43 (m, J = 6.6 Hz, 2H), 3.08 (t, J = 6 Hz, 2H), 6.97 (d, J = 7.2 Hz, 2H), 7.18 (m, 2H), 7.34 (m, J = 6.9 Hz, 2H), 7.58 (s, 1H), 7.64 (m, 1H), 8.14 (s, 1H); ^{13}C NMR (75 MHz, $CDCl_3$) 13.94, 20.11, 31.13, 43.25, 50.0, 50.05, 77.63, 115.75, 116.34, 118.46, 130.64, and 138.55.

To prepare AqB013, imidazolide of bumetanide (0.498 mmol) was added to a solution of 4-aminopyridine (0.996 mmol) and 1 ml of dry dichloromethane (argon atmosphere, 25°C), yielding a white precipitate. The mixture was diluted with 15 ml of EtOAc, transferred to a separatory funnel, and washed with water and then brine. The organic layer was removed, dried over $MgSO_4$, filtered, and concentrated under vacuum to obtain a yellowish white solid. The following results were obtained while verifying the preparation of AqB013: ^{1}H NMR (300 MHz, CD_3OD): 0.75 ppm (t, J = 5.4Hz, 3H), 1.10 ppm (m, 2H), 1.30 ppm (m, 2H), 2.85 ppm (t, br, 2H), 6.76 ppm (dd, 2H), 7.02 ppm (t, br, J = 6.9Hz, 1H), 8.00 ppm (d, J = 6.6Hz, 1H); ^{13}C NMR (75MHz, DMSO-d_6) 15.52, 22.26, 33.62, 45.27, 56.23, 111.56, 117.75, 131.89, 139.31, 142.72, 144.04, 159.54, and 163.02.

Intracellular Electrophysiological Recordings from Intact Gastric Antrum Preparations. Male C57BL6 mice (2–5 months of age) were anesthetized with CO_2 and killed by cervical dislocation. Stomachs were removed and opened along the lesser curvature. Luminal contents were washed away with Krebs-Ringer-bicarbonate solution (KRB) containing 120.7 mM NaCl, 15.5 mM $NaHCO_3$, 1.2 mM NaH_2PO_4, 5.9 mM KCl, 1.2 mM $MgCl_2$, 2.5 mM $CaCl_2$, and 11.5 mM dextrose. Tissues were pinned to the base of a Sylgard dish, and the mucosa of the antral region was removed by sharp dissection. The entire antral region of the murine stomach (5 × 8 mm), devoid of mucosa, was pinned to the floor of a recording chamber lined with Sylgard elastomer (Dow Corning, Midland, MI) with the circular layer facing upwards. Circular muscle cells were impaled with glass microelectrodes filled with 3 M KCl that had a resistance of 70 to 110 MΩ. Transmembrane potentials were amplified using an Axoclamp 2A amplifier (Molecular Devices, Sunnyvale, CA), digitized, and stored on a computer. Preparations were constantly perfused with oxygenated KRB warmed to 37°C. Nifedipine (1.0 μM), which has been shown not to significantly affect the wave form of antral regenerative potentials, was added to the KRB to suppress muscle movements.

Results

Bumetanide Reduces AQP4 Osmotic Water Flux. Osmotic water permeability of AQP4-expressing *X. laevis* oocytes is reduced by extracellular bumetanide but not by torsemide at concentrations up to 1 mM (Fig. 1). Effects of the loop diuretic compounds on the water permeability of AQP4-expressing oocytes were evaluated by osmotic swelling assays after preincubation in isotonic saline alone (untreated wild type) or in saline-containing bumetanide or torsemide (Fig. 1, a and b). A dose-response relationship shows a decrease in AQP4-mediated osmotic swelling by extracellular bumetanide at concentrations ≥100 μM (Fig. 1c). The inability of extracellular torsemide to block swelling at concentrations up to 1 mM (Fig. 1d) showed that indirect actions on an endogenous cotransporter cannot account for the observed block of water permeability by bumetanide. Furosemide applied extracellularly at concentrations up to 0.5 mM similarly was ineffective in blocking osmotic water permeability in AQP4-expressing oocytes (data not shown). The order of loop diuretic potencies distinguishes the block of AQP4 from possible effects on the endogenous *X. laevis* cotransporter, which has IC_{50} values of 2.5 μM for furosemide and less than 1 μM for bumetanide (Suvitayavat et al., 1994). Control (sham-

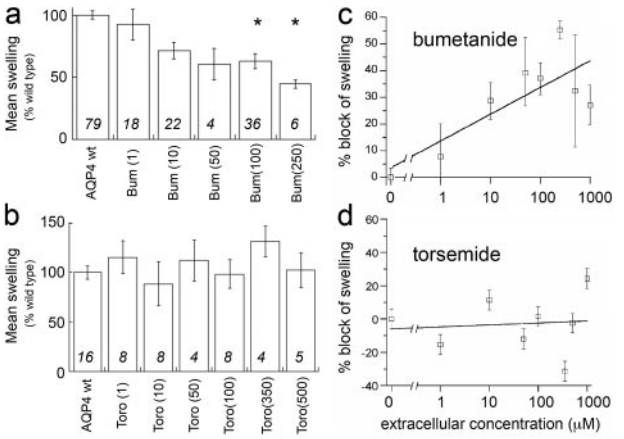

Fig. 1. Block of osmotic water permeability of AQP4-expressing *X. laevis* oocytes by extracellular bumetanide but not torsemide. Swelling rates were standardized to the mean rate of swelling for oocytes with untreated AQP4 wild-type channels set as 100% from the same experiment to allow the compilation of data across batches of oocytes. Doses of bumetanide (Bum; a) and torsemide (Toro; b) were applied extracellularly in isotonic saline at the doses indicated on the *x*-axis in parentheses (micromolar) 1 to 2 h before measurement of swelling rate in 50% hypotonic saline without drug. The threshold dose of bumetanide needed for statistically significant block ($p < 0.05$) was 100 μM (analysis of variance, post hoc Student's *t* test). Torsemide had no statistically significant effect on swelling rate, ruling out an appreciable contribution of endogenous cotransporters that are sensitive to loop diuretic drugs. Data are the mean ± S.E.M.; *n* values are in italics above the *x*-axis.

injected) oocytes were resistant to osmotically induced swelling and were not affected by the presence of loop diuretic drugs.

Identification of Intracellular Binding Sites. Putative binding sites on the AQP4 subunit for bumetanide and derivatives were proposed based on structural modeling and docking analyses (Fig. 2). Three discrete computational steps were used in this work: homology model preparation, binding site identification, and molecular docking studies. First, a homology model of rat AQP was derived from the bovine AQP1 crystal structure (Sui et al., 2001) deposited in the Protein Data Bank. Superimposed structures of bAQP1 crystal structure and the homology model of rAQP4 illustrate structural conservation of the subunit backbone (Fig. 2a), further confirmed by comparison of our rat AQP4 homology model with the human AQP4 electron crystal structure (Hiroaki et al., 2006) (data not shown). Second, in silico analyses were used to resolve three putative binding site cavities: two on the intracellular side of the AQP4 subunit, labeled sites 1 and 2, and one extracellular labeled site 3 (Fig. 2b). Sites 1 and 3 are located in water pore vestibules, and site 2 is a pocket formed by structural elements including the carboxyl terminus and intracellular loops of the protein. The possibility of an intracellular site of action implied by sites 1 and 2 was tested by direct injection of the loop diuretic compounds into AQP4-expressing oocytes before the swelling assays. Third, docking studies provided putative poses for the interaction of bumetanide and its derivatives with protein binding sites. These poses were used to suggest AQP4 amino acid residues for site-directed mutation studies and guide AqB chemical modifications in the development of potential ligand molecules.

In contrast to the modest blocking effect of extracellular bumetanide and lack of effect of extracellular furosemide, an increased efficacy of block was observed for both compounds after intracellular delivery via injection into AQP4-expressing oocytes (Fig. 3). Intracellular bumetanide yielded detectable block at 15 μM and significant block at 50 μM. Intracellular furosemide was more potent than bumetanide, with significant block observed at 5 μM and greater (Fig. 3a). The emergent blocking effect of intracellular furosemide and the enhanced efficacy of bumetanide after injection are observations consistent with an internal site of action, thus prioritizing candidate intracellular sites 1 and 2 while minimizing a possible role for extracellular site 3 for these drug agents. A lack of effect of external furosemide and torsemide is consistent with lower lipophilicities compared with bumetanide; the ClogP value (calculated log of the partition coefficient calculated as the ratio of the concentration of a compound in a nonaqueous solvent to the concentration in aqueous solution) is 3.40 for bumetanide, −0.83 for furosemide, and +0.47 for torsemide. It is possible that injected torsemide could also block water permeability; this was not tested, because data in hand showed that synthetic derivatives with increased membrane permeability were the preferred focus for further development.

Computational docking at intracellular candidate binding sites 1 and 2 (Fig. 2c) predicts H-bond, electrostatic, and hydrophobic interactions. At site 1, bumetanide docking is predicted to involve H-bond formation with the sulfonamide NH_2 moiety and hydrophobic surface interactions at the entrance to the AQP4 water pore. At site 2, a combination of H-bond donor and electrostatic interactions with the AQP4 residue Arg261 are implicated, as well as occupation of a deep hydrophobic pocket by the phenoxy substituent of bumetanide. Taken together, these results indicated that the core sulfamoyl benzoic acid scaffold shared by bumetanide and furosemide (Fig. 3b) was likely to be an important pharmacophore element and that improvements in membrane permeability were important properties to consider in designing synthetic derivatives. We developed a series of compounds engineered on the core structures of bumetanide and furosemide and tested them for possible blocking effects.

Enhanced Efficacy of Block by a Novel Bumetanide Derivative, AqB013. Significant block of AQP1- and AQP4-

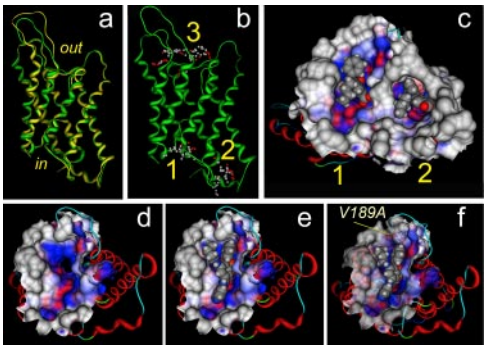

Fig. 2. Localization in silico of candidate binding sites for bumetanide and the more potent derivative AqB013 in a protein structural model of rat AQP4. a, structural homology model of rat AQP4 (green ribbon) superimposed on the crystal structure of bovine AQP1 (yellow ribbon). b, putative binding sites for bumetanide in AQP4 at intracellular sites 1 and 2 and extracellular site 3. c, docked poses of bumetanide (space-filling representation) in putative intracellular binding sites 1 and 2. The analytical Connolly solvent-accessible surface (solid surface) was computed for atoms within a radius of 9.0 Å around posed bumetanide to show the binding pockets. Colors reflect physicochemical properties of the surface around the ligand: hydrophobic (blue), hydrophilic (red), and solvent-exposed (gray). d, view of the wild-type AQP4 subunit seen from the intracellular side with the intrasubunit water pore in the center. e, docking of AqB013 at site 1 in the wild-type AQP4 subunit. f, docking of AqB013 at site 1 in AQP4 V189A subunit. The improved fit of the ligand suggests that the observed increase in efficacy of block (seen in swelling assays) could be due to reduced steric hindrance at the alanine residue (labeled position). For views d, e, and f, the analytical Connolly solvent-accessible surface (solid surface) was computed for atoms within a radius of 7.0 Å around site 1 α spheres.

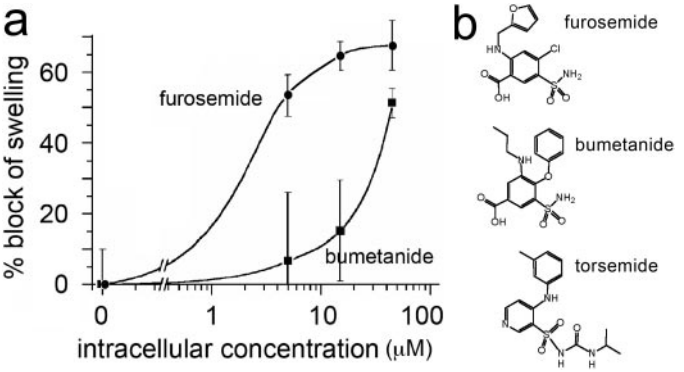

Fig. 3. Increased potency of block by intracellular delivery of bumetanide and furosemide via injection into AQP4-expressing oocytes. a, summary of the percentage block of swelling rates of AQP4-expressing oocytes after injection at 2 to 4 h before the swelling assay of a bolus volume (50 nl) of drug estimated to result in final intracellular concentrations of 0 to 100 μM (unpaired single swelling assays; see *Materials and Methods* for details). b, chemical structures of furosemide, bumetanide, and torsemide.

mediated osmotic water fluxes resulted from extracellular application of AqB013 (Fig. 4). Box plots show the swelling rate data collected for the double swelling protocol. AQP1- (Fig. 4a) or AQP4- (Fig. 4b) expressing oocytes were each tested in a first assay before treatment (first), and then incubated 1 to 2 h with AqB013 (0–100 μM) and subjected to a second swelling assay (second). Significant block was seen with external AqB013 at concentrations ≥20 μM (Fig. 4, a and b). The lack of a significant difference between the first and second swelling rates with no drug (0 μM) demonstrates that the initial swelling did not enhance or impair the subsequent response. A plot of paired data points for the first and second swelling rates per oocyte for a representative experiment (Fig. 4c) shows the slope of the linear relationship (m) is close to 1.0 for oocytes not treated with drug, as expected if the first and second swelling rates are comparable, and the slope was reduced more than 80% in the presence of the drug (AqB013, 50 μM), indicating block. Control oocytes showed little swelling and no appreciable effect of drug treatment (2 h, 50 μM). The blocking effect on AQP water permeability was dose-dependent and showed an IC_{50} value of approximately 20 μM for AQP1 and AQP4 (Fig. 4d), with maximal block at 50 μM. Mercuric ion at 50 μM was less potent than AqB013 in blocking AQP1, and as expected did not block mercury-insensitive AQP4 channels (Fig. 4e). These results identified AqB013 as an effective blocker for aquaporins.

Computational docking studies predicted AQP4 amino acids that could be involved in coordination of bumetanide binding (Fig. 2c), a subset of which were tested by site-directed mutagenesis (Fig. 5). The candidate residues of sites 1 and 2 were located mainly in intracellular loops B and D; site 2 also included the C-terminal end of AQP4, as illus-

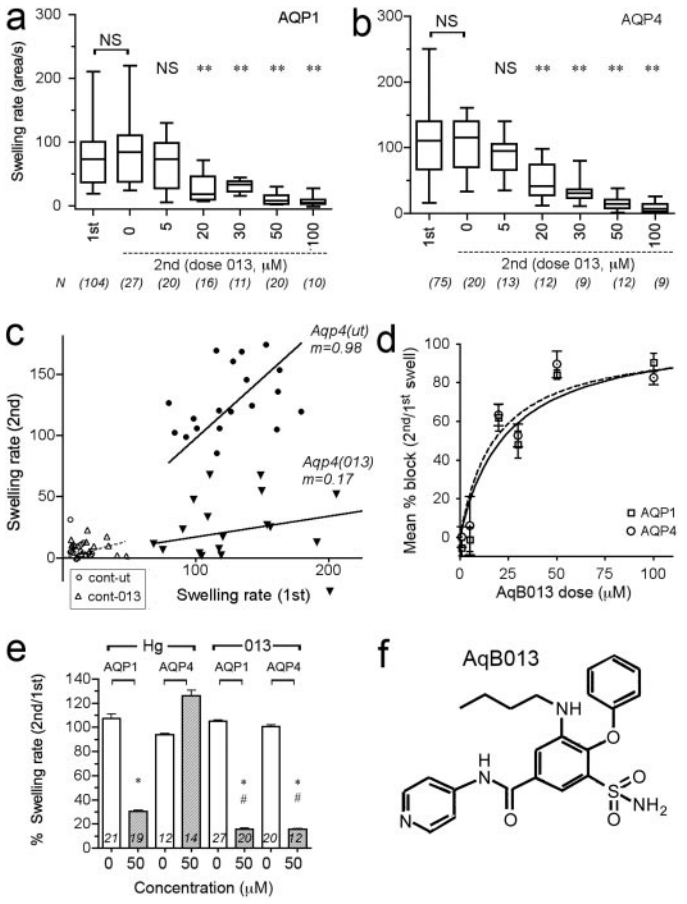

Fig. 4. Dose-dependent inhibition of AQP1- and AQP4-mediated osmotic swelling by extracellular application of a synthetic analog of bumetanide (AqB013). a and b, box plots show compiled data for the swelling rates measured in 50% hypotonic saline in an initial assay (first) and in a second assay after 1 to 2 h of incubation with the drug at the indicated dose (micromolar) for oocytes expressing AQP1 (a) and AQP4 (b). In the double-swelling assays, the first swelling was done before drug treatment; the second swelling for each individual oocyte was done after incubation in isotonic saline (untreated) or different doses of AqB013. c, plot of paired swelling rates for first and second swelling assays on the same oocytes, showing a linear relationship with a slope (m) near 1.0 for untreated and less than 1.0 for oocytes treated with 50 μM AqB013. Control oocytes (cont) showed little swelling and no apparent effect of the drug treatment. Oocytes were incubated for 1 to 2 h between paired swelling assays without drug (ut, untreated) or with drug (013) AqB013 at 50 μM. d, percentage of block calculated as $100(1.0 - (S2^{nd}/S1^{st}))$, where $S1^{st}$ is the initial swelling rate and $S2^{nd}$ is the second swelling rate for the same oocyte, and plotted as a function of drug dose (applied for the interval between the first and second assays). Data are mean ± S.E.M.; n values are as summarized in a and b. IC_{50} values were approximately 20 μM for both AQP1 and AQP4. e, compiled data for paired swelling rates ($100\% \times S2^{nd}/S1^{st}$) show the block of AQP1 but not AQP4 by mercuric chloride (50 μM) and effective block of both AQP1 and AQP4 by AqB013 at the same dose (50 μM). Data are the mean ± S.E.M.; n values in italics above x-axis. Statistically significant differences (analysis of variance, post hoc Bonferroni): *, $p < 0.05$ compared with matched untreated group; #, $p < 0.05$ compared with the level of block of AQP1 with mercury (Hg). f, chemical structure of AqB013.

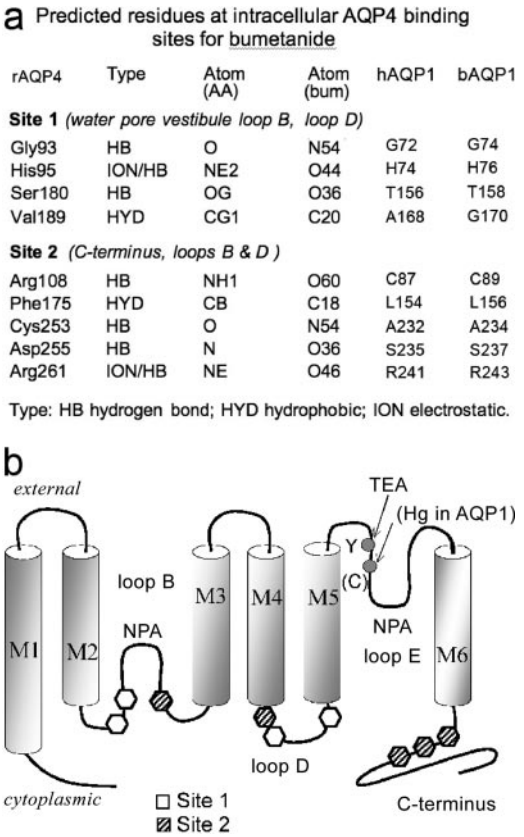

Fig. 5. Summary of the site 1 and site 2 amino acid residues predicted to interact with bumetanide. a, amino acid residues predicted by computational modeling to be involved in the binding of bumetanide derivatives at candidate sites 1 and 2 on the AQP4 subunit and the predicted nature of the interaction. The homologous residue in bovine (b) and human (h) AQP1 are listed (right columns). b, transmembrane topology diagram of an AQP subunit illustrating the positions of the residues of interest as potential contributors to the model-predicted sites 1 and 2 for bumetanide docking.

trated in a schematic transmembrane topology diagram (Fig. 5b).

AQP4 channels with site-directed mutations in sites 1 or 2 were tested in swelling assays with AqB013 at 50 μM (Fig. 6a). The mutations of Ser180 to arginine (S180R) and Val189 to alanine (V189A) both significantly enhanced the block by 50 μM AqB013 compared with the magnitude of block of wild-type AQP4 by AqB013, suggesting that modification of site 1 residues alters the potency of the drug effect. The lack of effect of site 2 mutations [Phe175 to alanine (F175A) and Arg261 to aspartic acid (R261D)] on the magnitude of block by 50 μM AqB013 indicates that a possible role of Site 2 is not apparent (or excluded), based on studies done thus far.

Specificity of the Block by AqB013. AqB013 has comparatively small or no effects on channel and transporter activities tested thus far (Fig. 7). Figure 7A shows that uptake of ^{86}Rb by human embryonic kidney cells expressing the human Na^+-K^+-$2Cl^-$ cotransporter hNKCC1 is blocked effectively by bumetanide as expected. The chemically related compound AqB013 has no effect on the cotransporter activity at 2 μM and causes approximately 20% block at 20 μM, demonstrating that the activity of the derivative has been shifted toward specificity for AQP, although the opportunity for further refinement remains. The block of the cotransporter by bumetanide is not affected by the presence of AqB013 coapplied in the flux assay saline. Figure 7B shows that endogenous chloride currents in *X. laevis* oocytes are not blocked by AqB013 (20 μM). Figure 7C shows that the solubilizing agent DMSO had no effect on osmotic swelling of oocytes at concentrations used in the drug assays. As a drug vehicle in the bumetanide assays, the highest concentration of DMSO used was 0.1% (v/v), a level that does not significantly affect the swelling response (Fig. 7c) and that is estimated to increase the osmolarity of the 50% hypotonic assay saline by less than 13%. DMSO in the AqB013 assays was ≤0.05%. The highest DMSO concentration (10%, 1.4 M) did cause shrinking attributed to strongly hypertonic osmotic pressure in the assay saline. Figure 7d shows that application of AqB013 (20 μM) via continuous perfusion in bath saline had no substantial effect on the rhythmic electrical conduction properties of ex vivo mouse antral gastric muscle compared with baseline before drug application and compared with recovery after washout. In the intact antral muscle, the addition of Aq013 did not change the resting membrane potential or the amplitude, frequency, or duration of slow waves, suggesting that the resting ionic conductances and the endogenous calcium, nonselective cation, and chloride conductances involved in pacing and generating slow waves (Takeda et al., 2008) are not appreciably affected by AqB013.

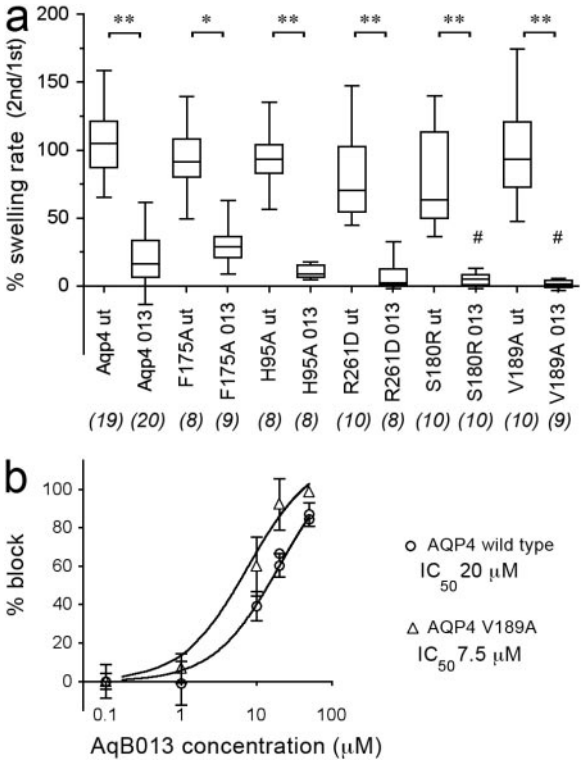

Fig. 6. Effects of mutations at sites 1 and 2 on the blocking effect of AqB013 on rat AQP4-mediated osmotic water permeability. a, summary of the effects of 50 μM AqB013 on osmotic swelling in 50% hypotonic saline for wild-type and mutant AQP4 channels modified by site-directed mutagenesis of residues modeled as possible contributors to sites 1 and 2 at the intracellular face (see Fig. 5 for reference). b, shift in the dose-response curve by mutagenesis of Val189 to alanine indicating an increased efficacy of block by AqB013 and implicating site 1 as a binding domain. The effect of the mutation on blocker efficacy confirms that action of the drug is on the AQP channel, not an endogenous oocyte protein.

Discussion

Our study was initiated to find selective agents capable of blocking water transport through aquaporins. Calls for the discovery of a blocker for AQP4 have been prompted by demonstrations of protective effects in cerebral edema in animal models that lack normal patterns of expression of brain AQP4, such as mice with deletions of AQP4 itself (Manley et al., 2000) or of scaffolding proteins such as α-syntrophin (Amiry-Moghaddam et al., 2004a,b) and dystrophin (Frigeri et al., 2001) that affect AQP4 expression and localization. A blocker of AQP4 is predicted to have a protective effect in edema after injury or stroke and would be attractive as a new clinical approach not only for brain injury but for many serious health concerns involving fluid imbalances.

Using bumetanide as a starting scaffold, we created a novel synthetic derivative, AqB013, and demonstrated that it is an effective inhibitor of AQP1 and AQP4. A direct action of AqB013 in AQP blockade is confirmed by results showing that mutation of specific amino acid residues in the predicted binding pocket (site 1 in the structural model of ligand-docking sites) increases sensitivity to AqB013. These data further suggest the intriguing idea that there is an internal regulatory binding pocket that modulates water permeability in AQP channels, perhaps involving a cytoplasmic ligand yet to be identified. The dose of 20 μM that causes half-maximal block in the oocyte expression system could be higher than that needed for blocking AQPs in mammalian cells, because *X. laevis* frog eggs have notably impermeant membranes even to agents considered to be membrane-permeable (Cooper and Boron, 1998).

Mutagenesis of the candidate binding site alters the efficacy of block. The site-directed mutation V189A in AQP4 shifted the dose-response relationship for block by AqB013 to the left (Fig. 6b), yielding an IC_{50} value of ~8 μM, significantly less than that seen for the wild-type AQP4 channel. The modeled effect of the mutation V189A on the molecular

docking of compound AqB013 in site 1 of AQP4 (and occlusion of the subunit water pore) is illustrated in Fig. 2. A potentiating effect of mutation V189A can be rationalized from the illustrated pose of AqB013 in site 1 (Fig. 2e), which suggests that the phenoxy substituent of bumetanide is better accommodated by the decrease in bulk when valine is substituted with the smaller alanine (Fig. 2f). An enhanced potency for block of wild-type hAQP1 might be expected compared with wild-type rAQP4, because the corresponding residue at the equivalent position in hAQP1 is alanine; however, the results did not distinguish any obvious differences in blocking efficacy, perhaps reflecting other structural considerations in the putative binding pockets.

The parsimonious interpretation of these data is that the water channel-blocking effect of bumetanide and analogs is occurring directly at the AQP itself at an intracellular binding pocket that allows direct occlusion of the pore. Furthermore, the blocking effect cannot be attributed to nonspecific actions on endogenous oocyte transporters. In summary, our results define a novel AQP blocking agent and show that the inhibitory action is influenced by subtle features of amino acids located on the cytoplasmic side of the AQP water channel pore in a putative binding pocket.

The inhibition by AqB013 of both AQP1 and AQP4 is consistent with results of structural modeling. For the candidate amino acids implicated in coordinating bumetanide binding, only minor topological differences exist in site 1 between bAQP1 and rAQP4. The two residues found thus far by mutagenesis to affect AqB013 efficacy are located in intracellular loop D, which has been proposed to serve in gating AQP channel functions in mammalian AQP1 (Yu et al., 2006), AQP4 (Fotiadis et al., 2002; Zelenina et al., 2002), and plant AQP (Tornroth-Horsefield et al., 2006). For these residues, Val189 of AQP4 is Gly170 in AQP1, and Ser180 in rAQP4 is Thr158 in bAQP1, which are conservative changes. Other site 1 residues are identical between AQP1 and -4; for example, in loop B on the N-terminal side of the signature NPA motif, Gly93 and His95 in AQP4 are Gly74 and His76 in bAQP1.

An allosteric modulatory role is possible for site 2 based on its location outside of the direct water pore pathway, but actions of bumetanide and its analogs at this site are not evident from results thus far. Site 2 is predicted to involve the C terminus, a region proposed in prior work to be involved in AQP1 regulation via Ca^{2+} binding (Fotiadis et al., 2002), and modulation of a cGMP-gated ionic conductance through the putative central pore of the tetrameric channel complex (Boassa and Yool, 2002, 2003; Yu et al., 2006; Yool, 2007a). The arginine residue in site 2 in the carboxyl terminus is conserved (243 in bAQP1; 261 in rAQP4). Additional residues for sites 1 and 2 involve intracellular loop B regions flanking the hairpin loop of the water pore (Jung et al., 1994b).

Unlike the Na^+-K^+-Cl^- transporter that is sensitive to block by membrane-permeable and -impermeable loop diuretics (Schlatter et al., 1983), activity of bumetanide and related compounds on AQP4 depends on intracellular delivery of the agent. A distinct mechanism of block by AqB013 is evident in three lines of evidence: 1) AqB013 is less effective than bumetanide in blocking NKCC1 transport and more effective than bumetanide in blocking AQP-mediated water flux; 2) AQP4 block is altered by mutation of a site 1 residue at the intracellular face of the water channel; and 3) loop diuretic agents with low lipid solubil-

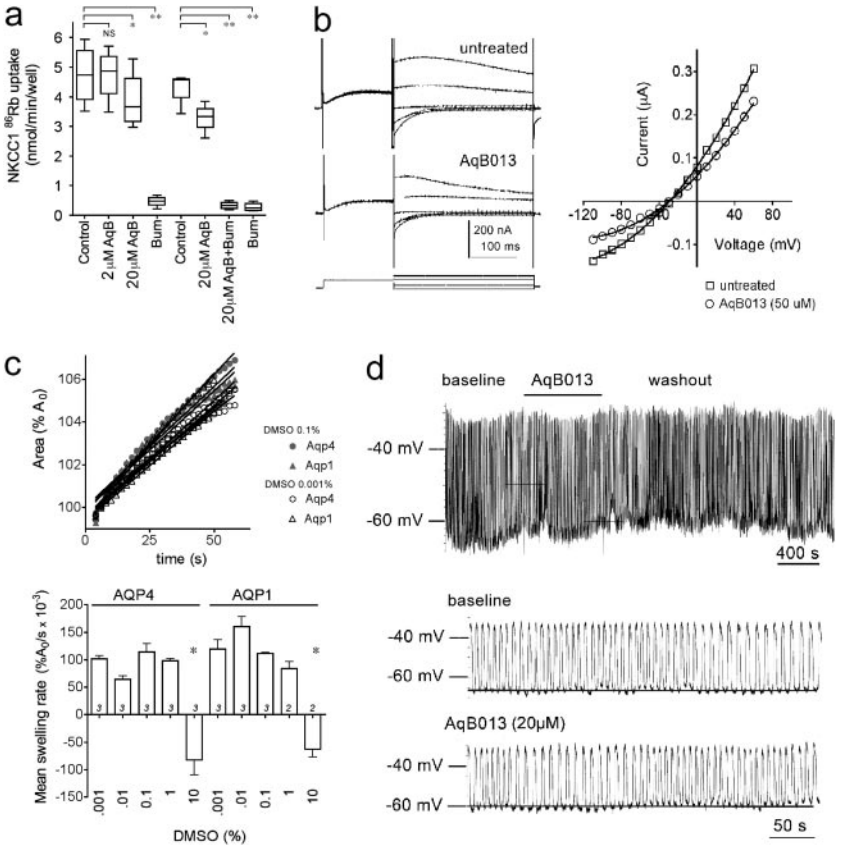

Fig. 7. Effect of AqB013 on the NKCC1 cotransporter (the target of the template compound bumetanide) or on several non-AQP classes of channels in situ. a, NKCC1-mediated ^{86}Rb flux is not blocked by AqB013 at 2 μM and is reduced by approximately 20% at 20 μM. Characteristic block of NKCC1 by bumetanide is retained in the presence of AqB013. b, endogenous chloride currents measured by two-electrode voltage clamp in *X. laevis* oocytes (left) in saline with 10 mM $CaCl_2$ are not affected by AqB013 (20 μM) and show comparable current-voltage relationships and reversal potentials (right). Voltage protocol: from a holding potential of -80 mV, voltage was stepped to -20 mV to enable Ca^{2+} entry, activating the Ca_{Cl} current, and then stepped to a range of voltages ($+40$ to -120 mV) to assess conductance. c, the drug-solubilizing vehicle DMSO has no effect on osmotic swelling of AQP1 or AQP4 expressing oocytes at doses $\leq$1% (v/v). Swelling is measured as the percentage of increase in cross-sectional area standardized to the initial area at time 0 (A_0) as a function of time after introduction into hypotonic saline (top). Swelling rates (slopes of the linear fits) are compiled as the mean $\pm$ S.E.M. (bottom). Only the highest concentration of DMSO (10%) had a significant effect on swelling. d, AqB013 (20 μM) does not alter the rhythmic electrical generation and conduction of slow waves in mouse gastric antral muscle.

ity (furosemide, torsemide) were ineffective when applied extracellularly at high concentrations. If the observed effect was due to Na^+-K^+-Cl^- cotransporter block, all of the loop diuretics should have influenced the oocyte swelling rates, because all were applied at doses exceeding characterized IC_{50} values. Structural modification of the carboxylic acid group of the bumetanide (as was done in creating the −013 derivative) is expected to decrease its effectiveness as a renal loop diuretic (Schlatter et al., 1983); this prediction is supported by our results. In summary, the AqB class of aquaporin blocking agents show a selectivity of action that holds promise for the development of targeted therapies.

AQP blockers have promise as a powerful adjunct for clinical intervention in stroke-related pathologies and relevance for a range of health concerns involving imbalances in fluid homeostasis. AQP4 channels localized in perivascular endfeet of astroglia in the central nervous system are proposed to serve physiologically as a route for the net movement of water out of the brain but in pathological conditions create vulnerability to cerebral edema, for example, after acute brain injury or stroke (Nico et al., 2003; Amiry-Moghaddam et al., 2004b; Puwarawuttipanit et al., 2006). Exciting opportunities await for testing AqB013 and related derivatives in disease models. With validation in vivo and the possibility of obtaining cocrystal structures with agents such as AqB013, the stage is set for the rational design of second-generation aquaporin modulators.

Acknowledgments

We thank Drs. G. M. Maggiora and B. Forbush for helpful discussions and A. Marble, L. O'Carroll, N. Fernando, R. L. Souza, and A. Citti for technical support.

References

Agre P, Preston GM, Smith BL, Jung JS, Raina S, Moon C, Guggino WB, and Nielsen S (1993) Aquaporin CHIP: the archetypal molecular water channel. *Am J Physiol* **265:**F463–F476.

Amiry-Moghaddam M, Frydenlund DS, and Ottersen OP (2004a) Anchoring of aquaporin-4 in brain: molecular mechanisms and implications for the physiology and pathophysiology of water transport. *Neuroscience* **129:**999–1010.

Amiry-Moghaddam M, Xue R, Haug FM, Neely JD, Bhardwaj A, Agre P, Adams ME, Froehner SC, Mori S, and Ottersen OP (2004b) Alpha-syntrophin deletion removes the perivascular but not endothelial pool of aquaporin-4 at the blood-brain barrier and delays the development of brain edema in an experimental model of acute hyponatremia. *FASEB J* **18:**542–544.

Boassa D and Yool AJ (2002) A fascinating tail: cGMP activation of aquaporin-1 ion channels. *Trends Pharmacol Sci* **23:**558–562.

Boassa D and Yool AJ (2003) Single amino acids in the carboxyl terminal domain of aquaporin-1 contribute to cGMP-dependent ion channel activation. *BMC Physiol* **3:**12.

Brooks HL, Regan JW, and Yool AJ (2000) Inhibition of aquaporin-1 water permeability by tetraethylammonium: involvement of the loop E pore region. *Mol Pharmacol* **57:**1021–1026.

Cooper GJ and Boron WF (1998) Effect of PCMBS on CO_2 permeability of *Xenopus* oocytes expressing aquaporin 1 or its C189S mutant. *Am J Physiol* **275:**C1481–C1486.

Darman RB and Forbush B (2002) A regulatory locus of phosphorylation in the N terminus of the Na-K-Cl cotransporter, NKCC1. *J Biol Chem* **277:**37542–37550.

Detmers FJ, de Groot BL, Müller EM, Hinton A, Konings IB, Sze M, Flitsch SL, Grubmüller H, and Deen PM (2006) Quaternary ammonium compounds as water channel blockers. Specificity, potency, and site of action. *J Biol Chem* **281:**14207–14214.

Edelsbrunner H, Facello M, Fu R, and Liang J (1995) Measuring proteins and voids in proteins, in *Proceedings of the 28th Annual Hawaii International Conference on System Sciences* (HICSS-28); 1995 Jan 3–6; Kihei, Maui, Hawaii; pp 256–264, IEEE Computer Society, Washington, DC.

Fotiadis D, Suda K, Tittmann P, Jenö P, Philippsen A, Müller DJ, Gross H, and Engel A (2002) Identification and structure of a putative Ca^{2+}-binding domain at the C terminus of AQP1. *J Mol Biol* **318:**1381–1394.

Frigeri A, Nicchia GP, Nico B, Quondamatteo F, Herken R, Roncali L, and Svelto M (2001) Aquaporin-4 deficiency in skeletal muscle and brain of dystrophic mdx mice. *FASEB J* **15:**90–98.

Hiroaki Y, Tani K, Kamegawa A, Gyobu N, Nishikawa K, Suzuki H, Walz T, Sasaki S, Mitsuoka K, Kimura K, et al. (2006) Implications of the aquaporin-4 structure on array formation and cell adhesion. *J Mol Biol* **355:**628–639.

Hohmann I, Bill RM, Kayingo I, and Prior BA (2000) Microbial MIP channels. *Trends Microbiol* **8:**33–38.

Huber VJ, Tsujita M, Kwee IL, and Nakada T (2009) Inhibition of Aquaporin 4 by antiepileptic drugs. *Bioorg Med Chem* **17:**418–424.

Jung JS, Bhat RV, Preston GM, Guggino WB, Baraban JM, and Agre P (1994a) Molecular characterization of an aquaporin cDNA from brain: candidate osmoreceptor and regulator of water balance. *Proc Natl Acad Sci U S A* **91:**13052–13056.

Jung JS, Preston GM, Smith BL, Guggino WB, and Agre P (1994b) Molecular structure of the water channel through aquaporin CHIP. The hourglass model. *J Biol Chem* **269:**14648–14654.

Lam TI, Anderson SE, Glaser N, and O'Donnell ME (2005) Bumetanide reduces cerebral edema formation in rats with diabetic ketoacidosis. *Diabetes* **54:**510–516.

Ma B, Xiang Y, Mu SM, Li T, Yu HM, and Li XJ (2004) Effects of acetazolamide and anordiol on osmotic water permeability in AQP1-cRNA injected *Xenopus* oocyte. *Acta Pharmacol Sin* **25:**90–97.

Manley GT, Fujimura M, Ma T, Noshita N, Filiz F, Bollen AW, Chan P, and Verkman AS (2000) Aquaporin-4 deletion in mice reduces brain edema after acute water intoxication and ischemic stroke. *Nat Med* **6:**159–163.

McClain RM and Dammers KD (1981) Toxicologic evaluation of bumetanide, potent diuretic agent. *J Clin Pharmacol* **21:**543–554.

Müller EM, Hub JS, Grubmüller H, and de Groot BL (2008) Is TEA an inhibitor for human Aquaporin-1? *Pflugers Arch* **456:**663–669.

Nico B, Frigeri A, Nicchia GP, Corsi P, Ribatti D, Quondamatteo F, Herken R, Girolamo F, Marzullo A, Svelto M, et al. (2003) Severe alterations of endothelial and glial cells in the blood-brain barrier of dystrophic mdx mice. *Glia* **42:**235–251.

Niemietz CM and Tyerman SD (2002) New potent inhibitors of aquaporins: silver and gold compounds inhibit aquaporins of plant and human origin. *FEBS letters* **531:**443–447.

O'Donnell ME, Tran L, Lam TI, Liu XB, and Anderson SE (2004) Bumetanide inhibition of the blood-brain barrier Na-K-Cl cotransporter reduces edema formation in the rat middle cerebral artery occlusion model of stroke. *J Cereb Blood Flow Metab* **24:**1046–1056.

Preston GM, Jung JS, Guggino WB, and Agre P (1993) The mercury-sensitive residue at cysteine 189 in the CHIP28 water channel. *J Biol Chem* **268:**17–20.

Puwarawuttipanit W, Bragg AD, Frydenlund DS, Mylonakou MN, Nagelhus EA, Peters MF, Kotchabhakdi N, Adams ME, Froehner SC, Haug FM, et al. (2006) Differential effect of alpha-syntrophin knockout on aquaporin-4 and Kir4.1 expression in retinal macroglial cells in mice. *Neuroscience* **137:**165–175.

Reizer J, Reizer A, and Saier MH Jr (1993) The MIP family of integral membrane channel proteins: sequence comparisons, evolutionary relationships, reconstructed pathway of evolution, and proposed functional differentiation of the two repeated halves of the proteins. *Crit Rev Biochem Mol Biol* **28:**235–257.

Schlatter E, Greger R, and Weidtke C (1983) Effect of "high ceiling" diuretics on active salt transport in the cortical thick ascending limb of Henle's loop of rabbit kidney. Correlation of chemical structure and inhibitory potency. *Pflugers Arch* **396:**210–217.

Sui H, Han BG, Lee JK, Walian P, and Jap BK (2001) Structural basis of water-specific transport through the AQP1 water channel. *Nature* **414:**872–878.

Suvitayavat W, Palfrey HC, Haas M, Dunham PB, Kalmar F, and Rao MC (1994) Characterization of the endogenous Na^+-K^+-$2Cl^-$ cotransporter in *Xenopus* oocytes. *Am J Physiol* **266:**C284–C292.

Takeda Y, Koh SD, Sanders KM, and Ward SM (2008) Differential expression of ionic conductances in interstitial cells of Cajal in the murine gastric antrum. *J Physiol* **586:**859–873.

Törnroth-Horsefield S, Wang Y, Hedfalk K, Johanson U, Karlsson M, Tajkhorshid E, Neutze R, and Kjellbom P (2006) Structural mechanism of plant aquaporin gating. *Nature* **439:**688–694.

Yang B, Kim JK, and Verkman AS (2006) Comparative efficacy of $HgCl_2$ with candidate aquaporin-1 inhibitors DMSO, gold, TEA^+ and acetazolamide. *FEBS Lett* **580:**6679–6684.

Yool AJ, Brokl OH, Pannabecker TL, Dantzler WH, and Stamer WD (2002) Tetraethylammonium block of water flux in Aquaporin-1 channels expressed in kidney thin limbs of Henle's loop and a kidney-derived cell line. *BMC Physiol* **2:**4.

Yool AJ (2007a) Aquaporins: multiple roles in the central nervous system. *Neuroscientist* **13:**470–485.

Yool AJ (2007b) Functional domains of aquaporin-1: keys to physiology, and targets for drug discovery. *Curr Pharm Des* **13:**3212–3221.

Yu J, Yool AJ, Schulten K, and Tajkhorshid E (2006) Mechanism of gating and ion conductivity of a possible tetrameric pore in aquaporin-1. *Structure* **14:**1411–1423.

Zelenina M, Zelenin S, Bondar AA, Brismar H, and Aperia A (2002) Water permeability of aquaporin-4 is decreased by protein kinase C and dopamine. *Am J Physiol Renal Physiol* **283:**F309–F318.

Address correspondence to: Dr. Andrea Yool, Discipline of Physiology, School of Molecular and Biomedical Science, Med School South Level 4 Frome Road, University of Adelaide, Adelaide SA 5005, Australia. E-mail: andrea.yool@adelaide.edu.au